Biochimica et Biophysica Acta 1837 (2014) 1730–1738

Contents lists available at ScienceDirect

Biochimica et Biophysica Acta

journal homepage: www.elsevier.com/locate/bbabio

Dynamics of the active site architecture in plant-type ferredoxin-NADP$^+$ reductases catalytic complexes

Ana Sánchez-Azqueta [a,b], Daniela L. Catalano-Dupuy [c], Arleth López-Rivero [c], María Laura Tondo [c], Elena G. Orellano [c], Eduardo A. Ceccarelli [c], Milagros Medina [a,b,*]

[a] Departamento de Bioquímica y Biología Molecular y Celular, Facultad de Ciencias, Universidad de Zaragoza, Zaragoza, Spain
[b] Instituto de Biocomputación y Física de Sistemas Complejos (BIFI), Unidad Asociada BIFI-IQFR (CSIC), Universidad de Zaragoza, Zaragoza, Spain
[c] Instituto de Biología Molecular y Celular de Rosario, CONICET, Facultad de Ciencias Bioquímicas y Farmacéuticas, Universidad Nacional de Rosario, Rosario, Santa Fe, Argentina

ARTICLE INFO

Article history:
Received 24 March 2014
Received in revised form 5 June 2014
Accepted 11 June 2014
Available online 20 June 2014

Keywords:
Ferredoxin-NADP$^+$ reductase
Flavoenzyme
Kinetic isotope effect
Hydride transfer
Charge–transfer complex
Plastidic-type FNR
Bacterial-type FPR

ABSTRACT

Kinetic isotope effects in reactions involving hydride transfer and their temperature dependence are powerful tools to explore dynamics of enzyme catalytic sites. In plant-type ferredoxin-NADP$^+$ reductases the FAD cofactor exchanges a hydride with the NADP(H) coenzyme. Rates for these processes are considerably faster for the plastidic members (FNR) of the family than for those belonging to the bacterial class (FPR). Hydride transfer (HT) and deuteride transfer (DT) rates for the NADP$^+$ coenzyme reduction of four plant-type FNRs (two representatives of the plastidic type FNRs and the other two from the bacterial class), and their temperature dependences are here examined applying a full tunnelling model with coupled environmental fluctuations. Parameters for the two plastidic FNRs confirm a tunnelling reaction with active dynamics contributions, but isotope effects on Arrhenius factors indicate a larger contribution for donor–acceptor distance (DAD) dynamics in the *Pisum sativum* FNR reaction than in the *Anabaena* FNR reaction. On the other hand, parameters for bacterial FPRs are consistent with passive environmental reorganisation movements dominating the HT coordinate and no contribution of DAD sampling or gating fluctuations. This indicates that active sites of FPRs are more organised and rigid than those of FNRs. These differences must be due to adaptation of the active sites and catalytic mechanisms to fulfil their particular metabolic roles, establishing a compromise between protein flexibility and functional optimisation. Analysis of site-directed mutants in plastidic enzymes additionally indicates the requirement of a minimal optimal architecture in the catalytic complex to provide a favourable gating contribution.
© 2014 Elsevier B.V. All rights reserved.

1. Introduction

Plant-type ferredoxin-NADP$^+$ reductases (FNRs) have evolved from a common ancestor into two classes: plastidic FNRs, which are found in plastids of plants, algae and cyanobacteria, and bacterial FNRs, herein known as FPRs [1,2]. The main role of plastidic FNR is the photosynthetic transfer of reduction equivalents from ferredoxin (Fd) to NADP$^+$ via its non-covalently bound FAD redox cofactor, although *in vivo* this reaction is reversible and FNR can provide electrons to different electron carrier proteins using NADPH as reductant [3]. The bacterial counterparts catalyse the non-photosynthetic reaction providing reducing power to detoxification and nitrogen fixation processes [1,2,4,5]. Differences in the requirements of their biological functions are reflected in turnover rates, substrate affinity and specificity, and, therefore, catalytic efficiency, as a result of the divergence achieved along functional specialisation. The lower catalytic efficiency of FPRs is related to structural differences in the isoalloxazine active site environment: i) the FAD acquires an extended conformation in plastidic FNRs but it is folded in FPRs and, ii) the isoalloxazine stacks between two Tyr residues (Tyr79 and the C-terminal Tyr303 in *Anabaena* (*An*FNR)) in plastidic FNRs, while FPRs

Abbreviations: FNR, ferredoxin-NADP$^+$ reductase; FPR, bacterial-type FNR; *An*FNR, FNR from the cyanobacterium *Anabaena* PCC 7119; *Ps*FNR, FNR from *Pisum sativum*; *Xa*FPR, FPR from *Xanthomonas axonopodis* pv. *citri*; *Ec*FPR, FPR from *Escherichia coli*; FNR_{ox}, FNR in the fully oxidised state; FNR_{hq}, FNR in the anionic hydroquinone (fully reduced) state; HT, hydride transfer; DT, deuteride transfer; WT, wild-type; CTC, charge–transfer complex; CTC-1, FNR_{ox}:NADPH CTC; CTC-2, FNR_{hq}:NADP$^+$ CTC; 2′-P-AMP, 2′-P-AMP moiety of NADP(H); N5-FAD, N5 hydride donor/acceptor of the FADH$^-$/FAD isoalloxazine ring of FNR; C4-NADP(H), C4 hydride acceptor/donor of the NADP$^+$/NADPH nicotinamide ring; NADPD, (4R)-4-^{2}H-NADPH; $k_{A\rightarrow B}$, $k_{B\rightarrow C}$, apparent/observed rate constants obtained by global analysis of spectral kinetic data; k_{HT}, k_{DT}, k_{obsHT}, k_{obsDT}, limiting hydride and deuteride transfer first-order rate constants for the reduction of FNR and their corresponding observed values under particular conditions; KIE, kinetic isotope effect on rate constants; A_H, A_D, Arrhenius pre-exponential factors for hydride and deuteride, respectively; E_{aH}, E_{aD}, activation energies for hydride transfer and deuteride transfer, respectively; DAD, donor–acceptor distance

* Corresponding author at: Departamento de Bioquímica y Biología Molecular y Celular, Facultad de Ciencias, Universidad de Zaragoza, E-50009 Zaragoza, Spain. Tel.: +34 976 762476; fax: +34 976 762123.
E-mail address: mmedina@unizar.es (M. Medina).

http://dx.doi.org/10.1016/j.bbabio.2014.06.003
0005-2728/© 2014 Elsevier B.V. All rights reserved.

have a C-terminal extension where the residue facing the isoalloxazine ring moiety is not the C-terminal [4,6–8] (Fig. 1). The length and sequence of this extension are not homogeneous among FPRs. Subclass I, including *Rhodobacter capsulatus* (*Rc*FPR) and *Xanthomonas axonopodis* pv. *citri* (*Xa*FPR) enzymes among others, has an Ala instead of the plastidic C-terminal Tyr followed by a Phe and up to 5 additional residues [9–12]. Members of subclass II maintain a Tyr stacking the *re*-face of the isoalloxazine and it is followed by a Trp, as in *Escherichia coli* FPR (*Ec*FPR) [13–15]. In both subclasses, the abovementioned Phe or Trp residue located at the C-terminal extension stacks on the adenosine moiety of FAD, apparently contributing to its folded conformation.

In plastidic FNRs the hydride transfer (HT) takes place between the N5 atom of the FAD(H^-) isoalloxazine (N5-FAD) and the C4 atom of the nicotinamide ring of NADP(H) (C4-NADP(H)) [16,17]. Mutational and theoretical analysis focused on the displacement of the Tyr stacking on the *re*-face of the isoalloxazine, required to allow the approaching of the reacting atoms during HT, have contributed to understand mechanistic details of this process as well as the role of the Tyr itself [17–26]. Though the presence of this Tyr is not obligatory for HT, it is crucial for the high catalytic efficiency of FNRs. It modulates the FAD midpoint reduction potential, avoids a too strong interaction between the reacting rings that would be incompatible with product release, and contributes to the optimal geometry between the reacting atoms for HT, N5-FAD and C4-NADP(H). Finally, it provides the active site with the required flexibility to allow the HT step occurring through tunnelling [21,22]. It is accepted that in bacterial FPRs the HT also takes place between C4-NADP(H) and N5-FAD. However, differences in the side-chain stacking against the isoalloxazine and, particularly, the presence of the C-terminal extension suggest a more complex mechanism to attain the catalytically competent interaction (Fig. 1) [6,7,11,15,27]. So far, no details about structural arrangement and dynamics of the active site during catalysis in FPRs have been provided.

The importance of slow (ms to s) protein flexibility in substrate recognition and allosterism is widely accepted [28]. Faster (fs to ps) motions coupled to the chemical step have also been pointed as contributing to active site dynamics in enzyme catalysed reactions. Variations of the Eyring's Transition State Theory have been used to treat enzyme-catalysed reactions, including fast electron–proton coupled transfers [29–39]. The most recent approaches postulate HT processes as fully quantum-mechanical events modulated by dynamical motions of the active site environment within the "environmentally coupled full tunnelling model" that describes two types of protein motions putatively linked to catalysis: pre-organisation and reorganisation [40]. Pre-organisation motions are assumed to occur prior to the HT event, in the ps to ns time scale, and involve large regions of the protein. Reorganisation motions involve heavy atoms within the active site, and constitute fast (ps to fs) nuclear fluctuations. Despite evidences for a role of protein dynamics in accelerating HT reactions [41–44], their contribution to catalysis is still on debate [45]. Studies on dihydrofolate reductases and on some pyridine-nucleotide dependent

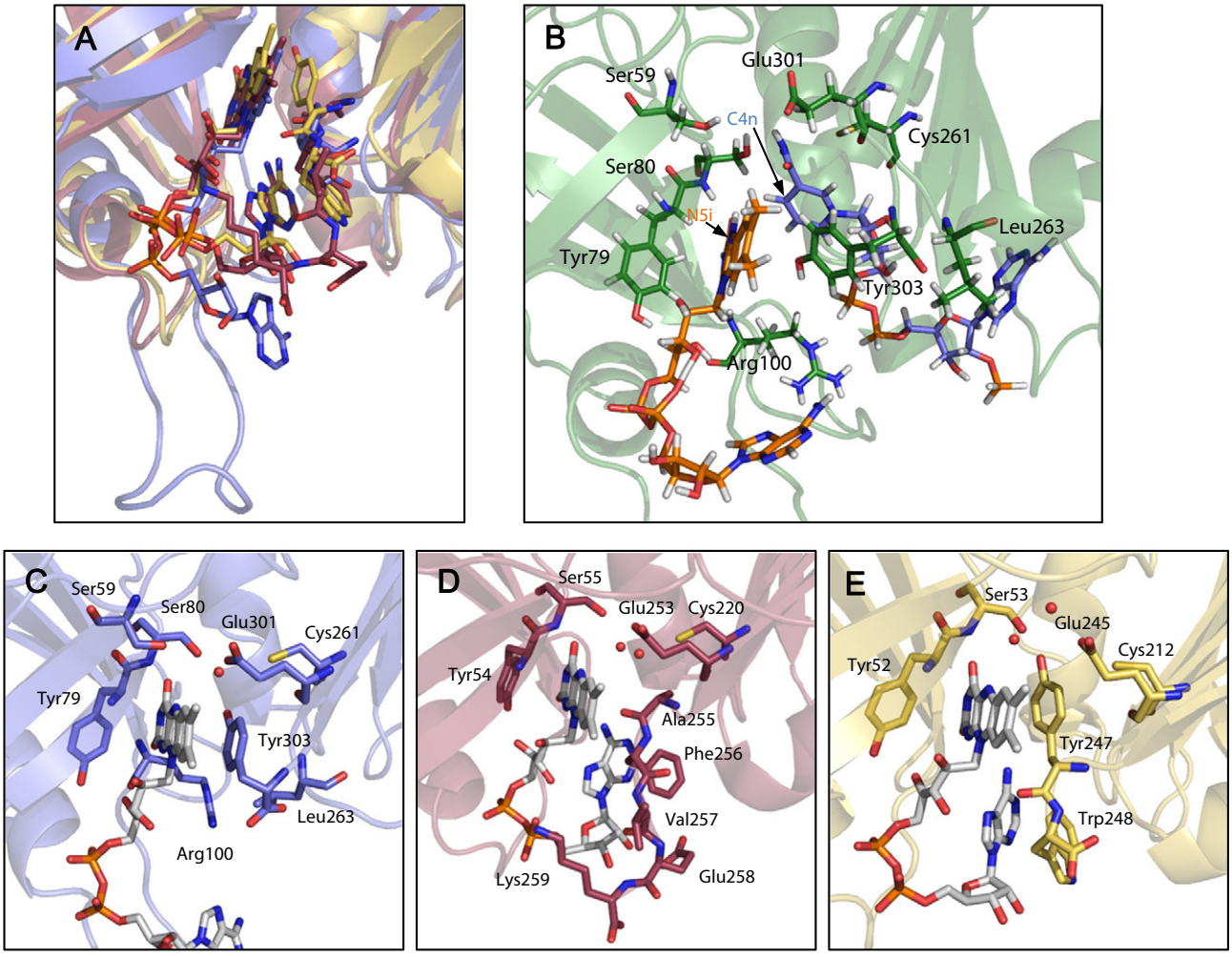

Fig. 1. The FAD environment in the plant-type FNR family. (A) Comparison of the FAD folding and environment in the crystal structures of *An*FNR (PDB 1que, blue), *Xa*FPR (PDB 4b4d, wine red) and *Ec*FPR (PDB 1fdr, yellow). (B) Theoretical model of the allocation of the nicotinamide moiety of $NADP^+$ in the active site of $AnFNR_{hq}$ as obtained by MD simulations [23]. Protein chain is shown in green, FAD in orange and NADPH in blue. Detail of the active site configuration in (C) *An*FNR, (D) *Xa*FPR and (E) *Ec*FPR. Key residues are shown as CPK coloured sticks.

flavoenzymes indicate that alterations of the active site environment and/or catalytic conditions lead to different dynamic behaviours [46,47]. Therefore, the ability of enzymes to undergo global (slow) rearrangements or local (fast) promoting vibrations appears to lead to some catalytic advantage, displaying a trend in which optimised active sites in native enzymes minimise donor–acceptor distance (DAD) fluctuations by attaining tunnelling ready geometries upon conformational sampling [34].

These methods have already been applied to investigate the plastidic-type *An*FNR [22,48]. In the present work, the analysis is extended to the HT processes of the plastidic *Pisum sativum* FNR (*Ps*FNR) and of the bacterial-type *Xa*FPR and *Ec*FPR, and the results compared with those of the *Anabaena* enzyme. The obtained data provide evidences to establish a divergent compromise between protein flexibility and functional optimisation. The study is completed with the characterization of several site-directed mutants in the plastidic *Ps*FNR contributing to a better understanding of the role of the active site environment architecture to attain optimal flexibility for HT.

2. Materials and methods

2.1. Biological material

Recombinant forms of *An*FNR, *Ps*FNR, *Ec*FPR and *Xa*FPR were produced and purified from *E. coli* cultures as previously reported [7,11,20,48–52]. Samples were prepared in 50 mM Tris/HCl, pH 8.0. (4R)-4-^{2}H-NADPH (herein NADPD, deuterium in the A face of the nicotinamide) was produced and purified as described [22,53]. For calculation of protein and NADP(H) concentrations by absorbance spectroscopy the following extinction coefficients were used: $\varepsilon_{460\ nm} = 9.7\ mM^{-1}\cdot cm^{-1}$ for *Ps*FNR (values for the mutants were 10.7, 11.3, 11.2, 11.1 and 10.7 $mM^{-1}\cdot cm^{-1}$ respectively for C266A, C266L, C266M, L268V and C266AL268V) [50], $\varepsilon_{450\ nm} = 10.7\ mM^{-1}\cdot cm^{-1}$ for *Xa*FPR [54], $\varepsilon_{460\ nm} = 9.7\ mM^{-1}\cdot cm^{-1}$ for *Ec*FPR [7], $\varepsilon_{260\ nm} = 18.0\ mM^{-1}\cdot cm^{-1}$ for $NADP^+$ (Sigma) and $\varepsilon_{340\ nm} = 6.22\ mM^{-1}\cdot cm^{-1}$ for NADPH (Sigma).

2.2. Stopped-flow pre-steady-state kinetic measurements

Fast HT reactions from NADPH to *Xa*FPR$_{ox}$ and *Ec*FPR$_{ox}$, as well as from *Xa*FPR$_{hq}$ and *Ec*FPR$_{hq}$ to $NADP^+$, were measured using a stopped-flow spectrophotometer from Applied Photophysics (SX.18MV, *Appl. Phot. Ltd.*) equipped with a photodiode array detector as previously described [48]. Measurements were carried out using 10 μM *Xa*FPR$_{ox/hq}$ or 7.5 μM *Ec*FPR$_{ox/hq}$ and NADP(H) in a 1:1–1:15 FPR:NADPH concentration ratio range, in 50 mM Tris/HCl, pH 8.0 at 25 °C and/or 6 °C. Multiple wavelength absorption data in the flavin absorption region (400–900 nm) were collected and processed using the X-Scan software (*Appl. Phot. Ltd.*). Time spectral deconvolution was performed by global analysis and numerical integration methods using Pro-Kineticist (*Appl. Phot. Ltd.*). Collected data were best fit to a single step A → B (or B → C) model allowing estimation of the conversion rate constants ($k_{A\rightarrow B}$ or $k_{B\rightarrow C}$) at each nucleotide concentration. Model validity was assessed by lack of systematic deviations from residual plots at different wavelengths, inspection of calculated spectra and consistence among the number of significant singular values with the fit model. When apparent rate constants were a function of coenzyme concentration, limiting values were estimated by data fitting to the reaction mechanism including all the experimental data for processes in both directions, considering the forward (k_{HT}) and reverse (k_{HT-1}) HT at equilibrium as previously described [48,55,56]. Errors in the estimated k_{HT} values were below ±10% in those cases were the reverse process was negligible, but might increase up to 35% when the reverse reaction was fast.

For accurate estimation of the non-photosynthetic HT or DT observed rate constants (k_{obsHT} or k_{obsDT}) from NADPH/D to the different reductases at different temperatures, single-wavelength kinetic traces were also followed. Traces at flavin band-I absorbance maxima (between 450 and 461 nm depending on the species) were recorded with a single-wavelength monochromator using the SX18.MV software (*App. Photo. Ltd.*) [22], and fitted to exponential decays by using the same software. Solutions of 10 μM of the corresponding FNR or FPR were mixed with the same concentrations of either NADPH or NADPD, with the exception of C266A *Ps*FNR, in which k_{obsHT} saturation dependence on the coenzyme concentration indicated that a 1:10 ratio was required for saturation [57]. Reactions were assayed at different temperatures between 5.3 and 17.3 °C. Traces for the reduction of *Ps*FNR, *Xa*FPR and *Ec*FPR fitted to monoexponentials (as reported for *An*FNR), therefore, determining k_{obsHT} and k_{obsDT} with errors estimated below ±10%.

Kinetic isotope effects on rate constants were calculated as

$$KIE = \frac{k_{obsHT}}{k_{obsDT}}. \quad (1)$$

For each isotope, fitting the observed rates to the Arrhenius equation

$$k = A * e^{-\frac{Ea}{RT}} \quad (2)$$

allowed the determination of the corresponding Arrhenius pre-exponential factors (A_H and A_D) and activation energy values (E_{aH} and E_{aD}). Combination of Eqs. (1) and (2) leads to the graphic representation of the temperature dependence of the KIE.

3. Results

3.1. Intermediate species during HT from NADPH to XaFPR and EcFPR

Previous analyses indicated that the HT process from NADPH to both *An*FNR and *Ps*FNR occurs through stabilisation within the instrumental dead time of a FNR$_{ox}$:NADPH charge transfer complex (CTC-1, characterised by a peak at 600 nm) that subsequently evolves to a FNR$_{hq}$:$NADP^+$ (CTC-2, characterised by a broad band at 800 nm) concomitant with flavin reduction [22,57]. This last step includes the HT event and fits to a one-step model allowing calculation of an observed HT rate, $k_{B\rightarrow C}$, that was virtually independent on the NADPH concentration (Fig. SM2A). When similarly analysing the reduction of *Xa*FPR and *Ec*FPR by NADPH two behaviours were observed, both of them differing from plastidic FNRs. Reduction of *Xa*FPR produced a decrease in the flavin band-I (450 nm) consistent with FAD reduction and CTC-2 appearance, but with lack of stabilisation of the intermediate CTC-1 along the process (Fig. 2A). Spectral evolution fitted to a one-step model with $k_{A\rightarrow B}$ values independent on the NADPH concentration (Fig. SM2A). Moreover, the reverse reaction was undetectable under our measurement conditions; therefore it can be taken as irreversible (Fig. SM2A). Altogether these data allowed the establishment of limiting k_{HT} values of 48.7 s^{-1} and 105 s^{-1} for the reduction of *Xa*FPR at 6 °C and 25 °C, respectively. On the other hand, reduction of *Ec*FPR by the coenzyme occurred through formation of a CTC-1 within the instrumental dead time (a not measurable A → B step), followed by the HT step that involved disappearance of both the flavin band-I and the CTC-1 one without detection of CTC-2 along the whole process (Figs. 2B and SM2B). Recorded spectra fitted to a one-step process, being, therefore, $k_{B\rightarrow C}$ related with k_{obsHT}. Surprisingly, for *Ec*FPR this parameter suffered an unexpected strong decrease when measured to NADPH concentrations over a 1:1 *Ec*FPR$_{ox}$:NADPH ratio (Fig. SM2A). Additionally, this enzyme was able to efficiently catalyse the reverse reaction without stabilisation of any CTC (Fig. SM2C). Therefore, the measured $^{app}k_{obsHT}$ is a combination of the microscopic constants for the forward and reverse reactions and the inhibition by the excess of substrate [56]. Fig. SM2A and Table SM1 resume parameters for the fitting of the experimental data of *Ec*FPR to the cited model. Nevertheless, several facts indicate that data derived from these simulations (Table SM1) must be taken

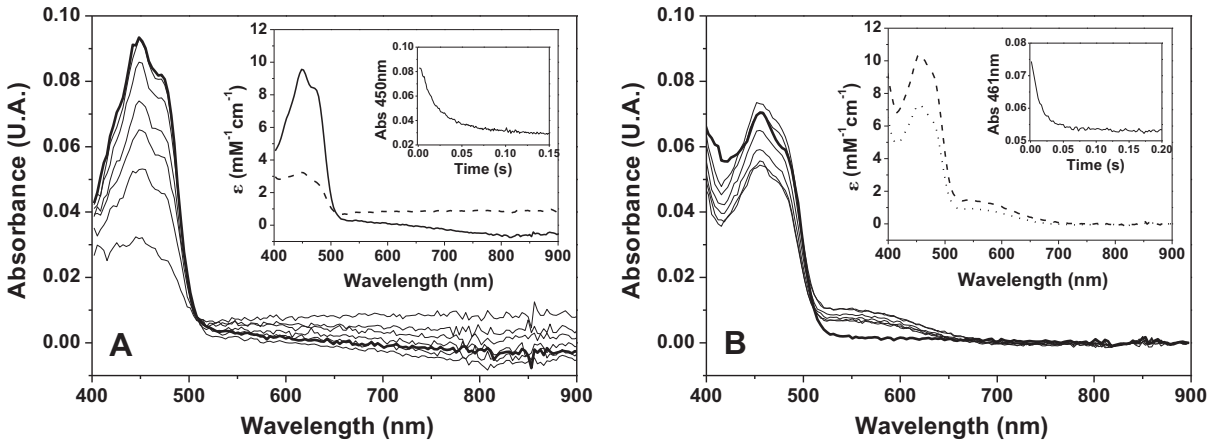

Fig. 2. Evolution of spectral changes during the reduction of bacterial FPRs by equimolecular concentrations of NADPH. (A) 10 μM *Xa*FPR, spectra recorded at 0.001 s, 0.005 s, 0.010 s, 0.015 s, 0.025 s and 0.15 s and (B) 7.5 μM *Ec*FPR, spectra recorded at 0.00384 s, 0.0064 s, 0.01152 s, 0.02432 s, 0.06272 s and 0.201 s. In all cases the thick spectra are the oxidised protein before mixing. The first inset shows absorbance spectra for the A (-), B (--) and C (···) species obtained by global analysis. The second inset shows time evolution of the absorbance maxima at 450 and 461 nm, respectively.

with caution and that other combination of parameters might fulfil the reaction: i) the number of parameters included as variables in the fitting is relatively high regarding the experimental data, ii) it is difficult to predict the difference in midpoint reduction potentials between the enzyme and the coenzyme once the complex is formed (surely they will change, since the redox equilibrium in Figs. 2B and SM2B indicates that the difference estimated from theoretical data is larger than the experimental one), and iii) the k_{HT-1} value seems to be too large against the $k_{obsHT-1}$ value derived from Fig. SM2C. When compared with plastidic FNRs, the k_{HT} values for the reduction of FPRs by NADPH are considerably lower (Tables 1 and 2).

3.2. KIE on the HT process and temperature effects

To investigate differences in active site organisation and dynamics during the HT event between plastidic- and bacterial-type FNRs, we applied the environmentally coupled tunnelling model for the determined KIEs on k_{obsHT} and k_{obsDT} at different temperatures (Fig. 3). Due to the reversibility of the process producing the apparent decrease in the experimentally measured rate constants upon increasing coenzyme concentration for *Ec*FPR reduction, equimolecular concentrations of enzyme and coenzyme were selected to further investigate this mechanism in all the species. A previous evaluation of *An*FNR showed moderate KIEs with relatively high E_a, suggesting that the tunnelling mediated process is more important for the lighter isotope [22] (Table 2). Additionally, the small ΔE_a ($E_{aD} - E_{aH}$) and the calculated isotope effect on the Arrhenius pre-exponential factor (A_H/A_D), which is near one, suggest transitions under the barrier. These results were explained as a full tunnelling process enhanced by both environmental heavy atom reorganisation (passive dynamics) and DAD fluctuations by vibrational modulation of the active site heavy atoms (known as active dynamics or "gating").

k_{obsHT} and k_{obsDT} have been similarly measured and analysed for *Ps*FNR, *Xa*FPR and *Ec*FPR. In all cases reduction by NADPD was slower than that by NADPH, producing similar or only slightly lower KIEs than those observed for *An*FNR (Table 2). *Ps*FNR k_{obsHT} and k_{obsDT} values showed less dependence than that of the *An*FNR, with their Arrhenius plots slightly deviating from parallel lines (Fig. 3A). This provided lower values for the E_a and pre-exponential factors for both isotopes, and produced a more significant decrease of KIE with temperature (Fig. 3B, Table 2). Therefore, ΔE_a and A_H/A_D resulted, respectively, larger than that for *An*FNR and very close to zero. These parameters remain indicative of protein dynamics contributions. Moreover, the greater the gating contribution, the more favourable HT compared to DT, meaning higher ΔE_a ($E_{aD} - E_{aH}$) and A_H/A_D ratios close to zero. This indicates that the gating enhancement dominates the HT global process in *Ps*FNR in much larger extension than in *An*FNR (as also inferred from the higher temperature dependence of the KIE).

The temperature dependence plots of k_{obsHT} and k_{obsDT} for the reduction of *Xa*FPR constituted two practically parallel lines, leading to almost temperature-independent KIEs, high E_a, $E_{aD} \approx E_{aH}$ and A_H/A_D considerably greater than the unity ($A_H/A_D = 10$) (Fig. 3A, Table 2). These parameters are consistent with passive environmental reorganisation movements dominating the HT step, and no contribution of DAD sampling or gating fluctuations. k_{obsHT} and k_{obsDT} temperature dependences for the reduction of *Ec*FPR also showed almost parallel lines at low temperatures. The considerably large value for the A_H/A_D ratio (150), and the temperature independent KIE at low temperatures were suggestive, as in *Xa*FPR, of heavy atom reorganisation dominating the reaction coordinate with undetectable gating contribution.

Table 1
HT rates and CTC detection during reduction of different plant-type FNRs by NADPH. Measurements carried out in 50 mM Tris/HCl, pH 8.0 at 6 °C with equimolar concentrations of protein and coenzyme. Evolution of the reaction was followed in a 400–1000 nm wavelength range using a stopped-flow equipped with a photodiode array detector.

FNR variant	k_{HT} (s^{-1})	CTC-1	CTC-2	C-ter architecture or ΔV[e]
*An*FNR[a]	300	Yes	Yes	—ET**Y**[f]
*Ps*FNR[b]	291	Yes	Yes	—EV**Y**
*Xa*FPR	48.7	No	Yes	—ER**A**FVEK
*Xa*FPR[c]	105	No	Yes	
*Ec*FPR[d]	64.0	Yes	No	—EH**Y**W
*Ps*L268V[b]	274	Yes	Yes	−25.0
*Ps*C266L[b]	0.49	No	No	53.2
*Ps*C266M[b]	0.14	No	No	55.5
*Ps*C266A[b]	27.1	No	No	−21.5
*Ps*C266AL268A[b]	0.86	No	No	−96.2

[a] Data from [22].
[b] Data from [57].
[c] Value obtained at 25 °C.
[d] Values obtained at 25 °C and corresponding to an apparent limiting $^{app}k_{obsHT}$ at a protein:coenzyme ratio 1:1.
[e] Volume change for *Ps*FNR mutants regarding the WT.

3.3. Role of the active site environment of plastidic-type FNR in the HT mechanism

Site-directed mutagenesis studies on the active site environment have been shown to alter stabilisation of intermediate CTC as well as to modulate HT rates in both FNRs and FPRs. In particular, changes in the amino acid volumes produce dramatic effects on HT and enzyme

Table 2
KIEs for the reduction of different plant-type FNRs.

FNR variant	HT (FNR_{ox} + NADPH)			DT (FNR_{ox} + NADPD)			KIE[a]	ΔE_a $E_{aD} - E_{aH}$ (kcal/mol)	A_H/A_D	Gating contribution
	k_{obsHT}[a] (s^{-1})	E_{aH} (kcal/mol)	A_H (s^{-1})	k_{obsDT}[a] (s^{-1})	E_{aD} (kcal/mol)	A_D (s^{-1})				
*An*FNR[b]	175 ± 1	12.8 ± 0.3	$1.8 \times 10^{12} \pm 0.4 \times 10^{12}$	27.0 ± 1.7	13.5 ± 0.6	$1.2 \times 10^{12} \pm 0.6 \times 10^{12}$	6.4 ± 0.5	0.7 ± 0.04	1.5 ± 0.5	+
*Ps*FNR	159 ± 14	6.0 ± 0.2	$8.2 \times 10^{6} \pm 0.4 \times 10^{6}$	38.6 ± 5.9	8.5 ± 0.5	$1.9 \times 10^{8} \pm 0.6 \times 10^{8}$	4.1 ± 0.7	2.5 ± 0.2	0.04 ± 0.01	++
*Xa*FPR	37.6 ± 1.2	17.7 ± 0.6	$2.8 \times 10^{15} \pm 0.6 \times 10^{15}$	7.9 ± 0.2	17.3 ± 0.5	$2.8 \times 10^{14} \pm 0.5 \times 10^{14}$	4.7 ± 0.2	−0.4 ± 0.02	10 ± 3.1	−
*Ec*FPR	7.8 ± 0.2	15.9 ± 0.4	$2.4 \times 10^{13} \pm 0.4 \times 10^{13}$	1.9 ± 0.1	13.8 ± 0.3	$1.3 \times 10^{11} \pm 0.4 \times 10^{11}$	4.1 ± 0.1	−2.1 ± 0.1	150 ± 47	−
*Ps*L268V	197 ± 9	6.3 ± 0.4	$1.7 \times 10^{7} \pm 0.5 \times 10^{7}$	31.7 ± 1.9	8.9 ± 0.5	$2.8 \times 10^{8} \pm 0.6 \times 10^{8}$	6.2 ± 0.5	2.6 ± 0.2	0.06 ± 0.02	++
*Ps*C266L	0.27 ± 0.01	16.2 ± 0.3	$1.3 \times 10^{12} \pm 0.4 \times 10^{12}$	n.d.	n.d.	n.d.	n.d.	n.d.	n.d.	n.d.
*Ps*C266M	0.15 ± 0.01	8.5 ± 0.7	$7.4 \times 10^{5} \pm 0.7 \times 10^{5}$	n.d.	n.d.	n.d.	n.d.	n.d.	n.d.	n.d.
*Ps*C266A[c]	1.63 ± 0.15	9.3 ± 0.2	$3.0 \times 10^{7} \pm 0.3 \times 10^{7}$	0.21 ± 0.01	10.6 ± 0.2	$4.5 \times 10^{7} \pm 0.3 \times 10^{7}$	7.9 ± 0.7	1.4 ± 0.04	0.67 ± 0.08	+
*Ps*C266AL268A	0.38 ± 0.06	13.4 ± 0.8	$9.6 \times 10^{9} \pm 0.7 \times 10^{9}$	0.09 ± 0.01	14.0 ± 1.7	$9.7 \times 10^{9} \pm 0.9 \times 10^{9}$	4.3 ± 1.0	0.6 ± 0.08	0.99 ± 0.12	+

[a] Values obtained in a stopped-flow equipment at 5.3 °C with equimolar concentrations of protein and coenzyme. Evolution of the reaction was followed at a single wavelength using the maximum of the flavin band-I.
[b] Data from [22].
[c] 1:10 ratio FNR:NADPH(D) was used to ensure saturation conditions.

catalysis [57,58]. The effects of these mutations on KIEs have only been reported for some *An*FNR variants [22,48,55], supporting the notion that changes of side-chain volumes in the flavin environment have strong influence in attaining the substrate:enzyme tunnel ready conformation [22,48]. We have analysed here the KIEs on k_{obsHT} and k_{obsDT} and their temperature dependences in several *Ps*FNR mutants to investigate the influence of the volume of residues interacting with the nicotinamide moiety of the coenzyme in the HT mechanism; namely L268V, C266L, C266M, C266A and C266AL268A [50,57] (Fig. 4). Parameters obtained upon analysis of L268V *Ps*FNR were very similar to those of WT *Ps*FNR (Table 2), indicating that this mutation has minor effects in the enzyme ability to bring the reacting atoms to tunnelling distance by vibrational enhancement. The C266M and C266L mutations produced a considerably deleterious effect on k_{obsHT} and increased the E_{aH} relative to the WT enzyme, additionally preventing reduction by NADPD at all assayed temperatures. Therefore, analyses on KIEs were not possible and only tunnelling of hydride, if any, might be taking place, thus discarding any observable gating enhancement.

Reduction of the C266A and C266AL268A variants by NADPH [57] and, particularly, by NADPD occurred to very low extents, affecting the accuracy of the calculated rate constants. Additionally, reduction of C266A *Ps*FNR occurred through a three-steps model including final stabilisation of some semiquinone [57]. Since regarding flavin reduction the first step accounted for considerably less amplitude than the second, rates for the second one were used to calculate KIE and its temperature dependence. For both variants the k_{obsHT} and k_{obsDT} temperature dependence showed two almost parallel lines with similar E_a values and $A_H/A_D \approx 1$, this latter parameter indicating a diminished gating contribution than in the WT (Fig. 4, Table 2). Therefore, despite the considerable decrease in k_{obsHT} and k_{obsDT} and reduced gating contribution observed for these two *Ps*FNR variants, both reorganisation and DAD dynamics seem to assist the catalytic tunnelling event as in the WT.

4. Discussion

Catalytically efficient interactions involving FNRs and pyridine nucleotides can be monitored through the spectroscopic observation of intermediate CTCs [22,59,60]. Despite bacterial-type FPRs also stabilising similar CTC-1 and CTC-2 bands, apparently they do it in different ratios relative to plastidic FNRs (Fig. 2 and [22]). Therefore, differences in the geometric disposition of the reacting rings in the catalytically competent complexes might be expected. Subclass I FPRs, as *Xa*FPR (Fig. 2A) and *Rc*FPR [27] favour spectroscopic stabilisation of CTC-2 versus CTC-1 while *Ec*FPR (subclass II) does not stabilise CTC-2 at all. These situations compare with data previously reported upon replacements at the C-terminal Tyr of plastidic FNRs. Removal of the C-terminal Tyr in Y303S *An*FNR induced large CTC-2 stabilisation making this variant only able to catalyse the non-photosynthetic reaction [21,22]. This behaviour is similar to that observed in subclass I FPRs, having an aliphatic residue in the equivalent position (Figs. 1 and 2). On the other hand, when a Trp substitutes for Tyr303 in *An*FNR no CTC-2 stabilisation is observed [22], as observed for the *Ec*FPR process (Fig. 2B), indicating that CTC stabilisation appears to be related to the nature of residues at the *re*-face of the isoalloxazine, a position where the nicotinamide moiety of the coenzyme is expected to locate.

These distinct organisations agree with previous structural and binding analyses, which suggest differences between plastidic- and bacterial-type FNRs in both coenzyme approach and geometry of the reacting complexes [21,60–64]. Three steps were described for coenzyme binding in plastidic FNRs [61]: (i) recognition of the 2′P-AMP moiety of NADP(H) in its binding cavity and fitting of the 2′P-AMP and pyrophosphate moieties: a leading role of the adenosine moiety in this step has been confirmed [65] and induces (ii) the subsequent structural rearrangements that approach the nicotinamide ring towards the isoalloxazine one; and finally (iii), the entrance of the nicotinamide

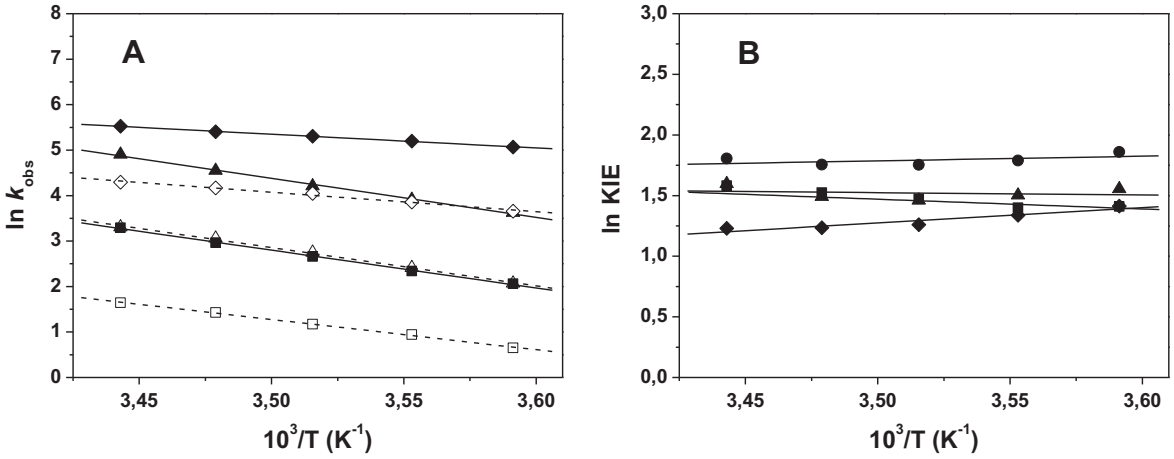

Fig. 3. Temperature dependence of kinetic parameters. (A) Arrhenius plots of kinetic constants for the reduction of *Ps*FNR (♦), *Xa*FPR (▲) and *Ec*FPR (■) by NADPH (closed symbols, solid line) and NADPD (open symbols, dashed line). (B) Temperature dependence of the KIEs for *An*FNR (●), *Ps*FNR (♦), *Xa*FPR (▲) and *Ec*FPR (■).

ring into the active site accompanied by displacement of the C-terminal Tyr which remains between the reacting rings to attain the catalytically isoalloxazine:nicotinamide competent geometry [23,24]. In bacterial FPRs displacement of the C-terminal extension is also expected to reach such a conformation. However, their 2′P-AMP binding region does not suffer major conformational changes upon coenzyme binding since the cavity is already preformed [15,27,66] and similar binding affinities are reported for $NADP^+$ and 2′P-AMP [6]. These two observations indicate that the entrance of the nicotinamide to the catalytic site is probably not promoted by binding at the 2′P-AMP site.

Relevance of dynamics of the C-terminal residue in plastidic FNR during catalysis was further proven by artificially reducing its mobility which severely affects the catalytic turnover [26]. The structure of bacterial FPRs fulfils the reduction of this motility by generating a more rigid C-terminus. Other types of pre-organisation motions could also explain low turnovers of FPRs. Thermal-activated conformational sampling represents slow to fast motions in which the protein–ligand complex samples a variety of conformations, some of which are able to support catalysis [42]. This might be relevant for *Xa*FPR and, particularly, *Ec*FPR. The latter catalyses the reverse reaction in large degree and suffers from product inhibition (Fig. SM2C and Table SM1). Moreover, large differences in binding affinity for the coenzyme can be rule out as responsible of the HT rate dependence with NADPH concentration, since previous K_d values for the interaction of the oxidised enzyme with $NADP^+$ were similar to those reported for other members of the family [7,11]. Instead, large protein fluctuations, particularly at the C-terminal extension, may contribute to increase the probability of attaining adequate nicotinamide:isoalloxazine fitting. These data, despite having no direct coupling to the HT reaction coordinate, reflect differences in pre-organisation motions to accommodate the substrate in the active site contributing to the overall catalytic enhancement of the process in plastidic enzymes compared to their bacterial counterparts.

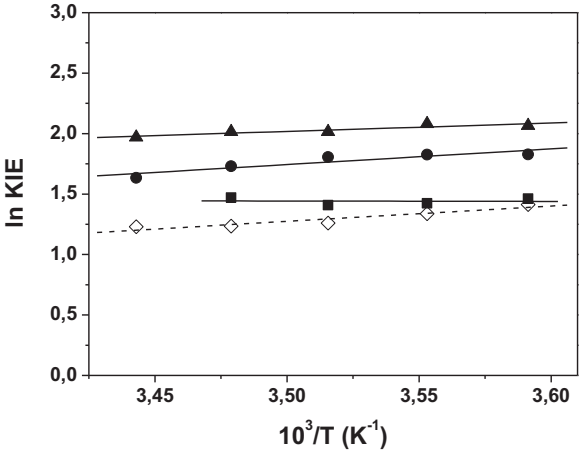

Fig. 4. Temperature dependence of the KIEs for WT (◊), L268V (●), C266A (▲) and C266AL268A (■) *Ps*FNRs.

Once the nicotinamide is in the active site, heavy atom reorganisation dynamics might additionally contribute to achieve a nuclear conformation suitable for tunnelling. KIEs, their temperature dependence and the data derived from the Arrhenius equation indicate that in *Ps*FNR HT occurs with an important tunnel contribution that relies on vibrational enhancement of the DAD to place the reacting atoms at optimal distance (Fig. 5), as reported for the cyanobacterial *An*FNR [22,48]. The gating component appears dominating more in *Ps*FNR than in *An*FNR, suggesting higher flexibility at the active site of the *Ps*FNR catalytically competent complex. This may relate to slight differences between cyanobacteria and higher plant FNRs in coenzyme occupancy of the active site, as described when binding was analysed by differential spectroscopy [65]. On the contrary, the data obtained for bacterial *Xa*FPR and *Ec*FPR, including temperature-independent KIEs and large A_H/A_D ratios, suggest that the initial pre-organisation situates the N5-FAD and C4-NADP(H) reacting atoms at optimal tunnel distance. This indicates that bacterial FPRs produce stiffer competent active sites than plastidic FNRs. In addition the E_{aH} values for bacterial FPRs were slightly higher, suggesting higher reorganisation energies as the main source of E_a. Therefore, it can be postulated that the role of FPRs as mediators in slow catalytic rate demanding metabolic chains made unnecessary, even undesirable, catalytic improvement. Thus, FPRs reached midpoint reduction potentials, protein interaction surfaces and nucleotide binding features compatible with their biological requirements, while FNRs needed a divergent development to fulfil the requirements of high demanding reaction rates linked to protein rearrangements to ensure optimal and quick discrimination between NADP/NAD or protein partners. Thus, active sites of plastidic FNRs evolved to achieve enhanced catalytic and HT rates, as well as quick dissociation of products to fulfil the photosynthesis needs. The suboptimal geometry for HT of plastidic FNRs after heavy atom reorganisation appears as a reasonable cost to compensate for all mentioned improvements. Thus, they subsequently require DAD sampling to reach the optimal tunnel conformation. Noticeably, gating contribution appears more important in *Ps*FNR than in *An*FNR, being the first also more efficient in terms of turnover rates. Recent studies hypothesise that protein evolution towards native enzymes attained well packed active sites displaying tunnelling ready conformations and minimisation of the

gating contribution [67]. According to the results presented here bacterial FPRs may be a good example of this.

Since the architecture of active sites is a key to assist both pre-organisation and reorganisation in the achievement of a tunnelling ready conformation, its modification can compromise optimal disposition of reacting atoms and increase DAD sampling to achieve it. In plastidic FNRs, either mutations at the active site or changing the volume at positions involved in nicotinamide allocation produced perturbations in CTC stabilisation during HT [22,48,50,57]. Among them, mutants at Leu268 and Cys266 in *Ps*FNR were designed to increment (C266M and C266L) or decrease (L268V, C266A and C266AL268A) the protein volume at the C-terminal Tyr side not facing the isoalloxazine [50]. Leu268 side-chain is situated behind it, but changes in its volume have no effects on HT rates, CTC formation or active site dynamics, indicating a minimal contribution to attain the catalytically complex geometry and to the HT itself, in agreement with it not interacting with any of the reacting rings during this event. On the contrary, obvious impairments of the stacking between the reacting rings, deduced from the absence of CTC and of HT efficiency, were observed for mutants at Cys266 [57]. In this line, theoretical studies predicted that the thiol group of this residue stabilises the C4-NADP(H) atom of the nicotinamide promoting the N5-FAD:C4-NADP(H) approach [23,24]. However, reduction of C266A and C266AL268A *Ps*FNR by NADPH still takes place through tunnelling but with a gating contribution to the tunnel somehow diminished regarding the WT (Fig. 4). This later observation can be related to reduction of the nicotinamide constraint against the isoalloxazine and to the lack of the interaction between the thiol of Cys266 and the C4-NADP(H), thus hampering the efficient ring orientation. The new arrangement would generate a stiffer active site with a less dominant vibrational modulation of HT, as discussed for the thermophilic alcohol dehydrogenase and the soybean lipoxygenase-I [32]. The increase of volume at position 266 in C266M and C266L *Ps*FNRs also led to a deleterious effect on HT, and, surprisingly, impaired DT (Table 2, Fig. 4). An explanation to the low HT efficiency and lack of DT entails the assumption that, in the final isoalloxazine:nicotinamide complex the N5-FAD and C4-NADP(H) atoms remain so distant that the overlapping of the wave function is too small for hydrogen and negligible for deuterium (the smaller wavelength of deuterium compared to hydrogen makes it tunnelling at smaller DAD). In agreement, the structure of C266M *Ps*FNR showed a displacement of Glu306 away from Met266 and the key Ser90 that can lead to a hindered N5-FAD:C4-NADP(H) geometry [57]. Though our experimental results do not rule out gating contribution in this particular case, evidences indicate that for these mutants active site compression impedes DAD fluctuations. Reported KIEs in the non-photosynthetic HT reaction for several *An*FNR variants indicated that tunnel for WT and some mutants was contributed by both reorganisation energy and thermal compression of reacting atoms. For a second group of mutants, gatin appears to dominate the reaction coordinate. Finally, in a third group tunnelling ready geometries were achieved through reorganisation motions with no DAD vibrational enhancement [22,48,55,57]. Parameters for mutants at Cys266 in *Ps*FNR situate its replacement by Ala in the first group and by Met or Leu in the last one. However, compared with *An*FNR mutants the Cys266 ones considerably hinder the HT efficiency and the stabilisation of CTC. Therefore, the volume of the residue at position 266 is essential to attain the catalytic architecture between the nicotinamide and isoalloxazine rings at the active site and that reorganisation dynamics is not able to overcome the negative effects induced by changes in the volume of this side-chain.

5. Conclusions

Recent theories suggest small gating contributions for native enzymes in HT catalysed reactions where reorganisation movements of heavy atoms are enough to attain tunnel ready conformations [34,46]. This appears the case for bacterial FPRs, whereas DAD sampling is additionally required by the plastidic members of the family. The stiff active sites of bacterial FPRs appear perfectly adapted to the low demanding rates of the processes they participate in, while plastidic FNRs require gating to achieve tunnel ready conformations. These observations support the idea that bacterial and plastidic enzymes had evolved very early, each of them specialising according to their metabolic roles. Plastidic enzymes have achieved their high efficiencies in adaptation to the demanding functions they play: minimisation of DAD fluctuations might be an ultimate optimisation to overcome after all functionality needs are fulfilled. Active site substitutions in plastidic FNRs decreased DAD sampling by two main reasons: allocation of the nicotinamide with apparent optimal N5-FAD:C4-NADP(H) distance and, orientation or stiffness of the active site due to steric/energetic impediments that cause too high gating frequencies (as in Cys266 mutants). These second possibilities usually impair HT and, therefore, a decrease or lack of observable gating does not mean active site optimisation. Mutations can also generate non-optimal tunnelling distances between the exchanging atoms, making vibrations of the reacting atoms necessary to generate a suitable barrier for tunnelling. However, the analysed Cys266 mutants are not able to overcome the architecture impairment. In fact, mutations leading to more flexible active sites in *An*FNR and *Ps*FNR are catalytically more competent that could be expected from

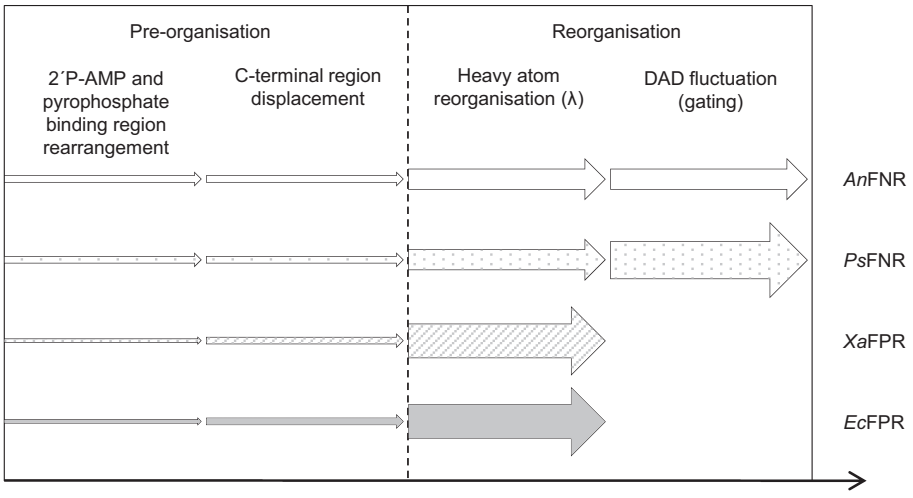

Fig. 5. Involvement of pre-organisation and reorganisation dynamics during the HT processes from the coenzyme to *An*FNR (solid white), *Ps*FNR (dotted), *Xa*FPR (striped) and *Ec*FPR (solid grey). Sizes of arrows only qualitatively indicate the contribution of each type of motion to catalysis.

their HT rates. Therefore, deviations from the general behaviour can be rationalised as an adaptive mechanism of enzymes for working under non-optimal situations, or for less ancient ones in which the cost for dynamics at active site compensates for an improvement in efficiency.

Acknowledgements

This work has been supported by MINECO, Spain (BIO2010-14983 and BIO2013-42978-P to M.M.), ANPCyT, Argentina (PICT 2010-1762 to E.G.O., PICT-2012-1841 to E.A.C. and 00739 to D.L.C.D.) and CONICET, Argentina (PIP 252 to E.A.C. and 114-200901-00337 to D.L.C.D.). A.S.-A. thanks a FPU fellowship from the Spanish Ministry of Education. A.L.R. and M.L.T. are fellows of the CONICET, Argentina.

Appendix A. Supplementary data

Supplementary data to this article can be found online at http://dx.doi.org/10.1016/j.bbabio.2014.06.003.

References

[1] A. Aliverti, V. Pandini, A. Pennati, M. de Rosa, G. Zanetti, Structural and functional diversity of ferredoxin-NADP$^+$ reductases, Arch. Biochem. Biophys. 474 (2008) 283–291.
[2] E.A. Ceccarelli, A.K. Arakaki, N. Cortez, N. Carrillo, Functional plasticity and catalytic efficiency in plant and bacterial ferredoxin-NADP(H) reductases, Biochim. Biophys. Acta 1698 (2004) 155–165.
[3] P. Razquin, M.F. Fillat, S. Schmitz, O. Stricker, H. Bohme, C. Gómez-Moreno, M.L. Peleato, Expression of ferredoxin-NADP$^+$ reductase in heterocysts from *Anabaena* sp. Biochem. J. 316 (Pt 1) (1996) 157–160.
[4] N. Carrillo, E.A. Ceccarelli, Open questions in ferredoxin-NADP$^+$ reductase catalytic mechanism, Eur. J. Biochem. 270 (2003) 1900–1915.
[5] M. Medina, C. Gómez-Moreno, Interaction of ferredoxin-NADP$^+$ reductase with its substrates: optimal interaction for efficient electron transfer, Photosynth. Res. 79 (2004) 113–131.
[6] I. Nogués, I. Pérez-Dorado, S. Frago, C. Bittel, S.G. Mayhew, C. Gómez-Moreno, J.A. Hermoso, M. Medina, N. Cortez, N. Carrillo, The ferredoxin-NADP(H) reductase from *Rhodobacter capsulatus*: molecular structure and catalytic mechanism, Biochemistry 44 (2005) 11730–11740.
[7] M.A. Musumeci, H. Botti, A. Buschiazzo, E.A. Ceccarelli, Swapping FAD binding motifs between plastidic and bacterial ferredoxin-NADP(H) reductases, Biochemistry 50 (2011) 2111–2122.
[8] J. Yeom, C.O. Jeon, E.L. Madsen, W. Park, Ferredoxin-NADP$^+$ reductase from *Pseudomonas putida* functions as a ferric reductase, J. Bacteriol. 191 (2009) 1472–1479.
[9] C. Bittel, L.C. Tabares, M. Armesto, N. Carrillo, N. Cortez, The oxidant-responsive diaphorase of *Rhodobacter capsulatus* is a ferredoxin (flavodoxin)-NADP(H) reductase, FEBS Lett. 553 (2003) 408–412.
[10] G. Sridhar Prasad, N. Kresge, A.B. Muhlberg, A. Shaw, Y.S. Jung, B.K. Burgess, C.D. Stout, The crystal structure of NADPH:ferredoxin reductase from *Azotobacter vinelandii*, Protein Sci. 7 (1998) 2541–2549.
[11] M.L. Tondo, M.A. Musumeci, M.L. Delprato, E.A. Ceccarelli, E.G. Orellano, Structural–functional characterization and physiological significance of ferredoxin-NADP$^+$ reductase from *Xanthomonas axonopodis* pv. *citri*, PLoS One 6 (2011) e27124.
[12] M.L. Tondo, R. Hurtado-Guerrero, E.A. Ceccarelli, M. Medina, E.G. Orellano, M. Martinez-Julvez, Crystal structure of the FAD-containing ferredoxin-NADP(+) reductase from the Plant pathogen *Xanthomonas axonopodis* pv. *citri*, Biomed. Res. Int. (2013) (2013) ID906572.
[13] M. Ingelman, V. Bianchi, H. Eklund, The three-dimensional structure of flavodoxin reductase from *Escherichia coli* at 1.7 Å resolution, J. Mol. Biol. 268 (1997) 147–157.
[14] A.R. Krapp, R.E. Rodríguez, H.O. Poli, D.H. Paladini, J.F. Palatnik, N. Carrillo, The flavoenzyme ferredoxin (flavodoxin)-NADP(H) reductase modulates NADP(H) homeostasis during the soxRS response of *Escherichia coli*, J. Bacteriol. 184 (2002) 1474–1480.
[15] J.T. Wan, J.T. Jarrett, Electron acceptor specificity of ferredoxin (flavodoxin):NADP$^+$ oxidoreductase from *Escherichia coli*, Arch. Biochem. Biophys. 406 (2002) 116–126.
[16] C.J. Batie, H. Kamin, Ferredoxin:NADP$^+$ oxidoreductase. Equilibria in binary and ternary complexes with NADP$^+$ and ferredoxin, J. Biol. Chem. 259 (1984) 8832–8839.
[17] M. Medina, Structural and mechanistic aspects of flavoproteins: photosynthetic electron transfer from photosystem I to NADP$^+$, FEBS J. 276 (2009) 3942–3958.
[18] Z. Deng, A. Aliverti, G. Zanetti, A.K. Arakaki, J. Ottado, E.G. Orellano, N.B. Calcaterra, E.A. Ceccarelli, N. Carrillo, P.A. Karplus, A productive NADP$^+$ binding mode of ferredoxin-NADP$^+$ reductase revealed by protein engineering and crystallographic studies, Nat. Struct. Biol. 6 (1999) 847–853.
[19] I. Nogués, J. Tejero, J.K. Hurley, D. Paladini, S. Frago, G. Tollin, S.G. Mayhew, C. Gómez-Moreno, E.A. Ceccarelli, N. Carrillo, M. Medina, Role of the C-terminal tyrosine of ferredoxin-nicotinamide adenine dinucleotide phosphate reductase in the electron transfer processes with its protein partners ferredoxin and flavodoxin, Biochemistry 43 (2004) 6127–6137.
[20] J. Tejero, I. Pérez-Dorado, C. Maya, M. Martínez-Júlvez, J. Sanz-Aparicio, C. Gómez-Moreno, J.A. Hermoso, M. Medina, C-terminal tyrosine of ferredoxin-NADP$^+$ reductase in hydride transfer processes with NAD(P)$^+$/H, Biochemistry 44 (2005) 13477–13490.
[21] I. Lans, J.R. Peregrina, M. Medina, M. García-Viloca, A. González-Lafont, J.M. Lluch, Mechanism of the hydride transfer between *Anabaena* Tyr303Ser FNR_{rd}/FNR_{ox} and NADP$^+$/H. A combined pre-steady-state kinetic/ensemble-averaged transition-state theory with multidimensional tunneling study, J. Phys. Chem. B 114 (2010) 3368–3379.
[22] J.R. Peregrina, A. Sánchez-Azqueta, B. Herguedas, M. Martínez-Júlvez, M. Medina, Role of specific residues in coenzyme binding, charge–transfer complex formation, and catalysis in *Anabaena* ferredoxin-NADP$^+$ reductase, Biochim. Biophys. Acta 1797 (2010) 1638–1646.
[23] J.R. Peregrina, I. Lans, M. Medina, The transient catalytically competent coenzyme allocation into the active site of *Anabaena* ferredoxin-NADP$^+$ reductase, Eur. Biophys. J. 41 (2012) 117–128.
[24] I. Lans, M. Medina, E. Rosta, G. Hummer, M. García-Viloca, J.M. Lluch, A. González-Lafont, Theoretical study of the mechanism of the hydride transfer between ferredoxin-NADP$^+$ reductase and NADP$^+$: the role of Tyr303, J. Am. Chem. Soc. 134 (2012) 20544–20553.
[25] L. Piubelli, A. Aliverti, A.K. Arakaki, N. Carrillo, E.A. Ceccarelli, P.A. Karplus, G. Zanetti, Competition between C-terminal tyrosine and nicotinamide modulates pyridine nucleotide affinity and specificity in plant ferredoxin-NADP$^+$ reductase, J. Biol. Chem. 275 (2000) 10472–10476.
[26] D.L. Catalano-Dupuy, M. Orecchia, D.V. Rial, E.A. Ceccarelli, Reduction of the pea ferredoxin-NADP(H) reductase catalytic efficiency by the structuring of a carboxyl-terminal artificial metal binding site, Biochemistry 45 (2006) 13899–13909.
[27] A. Bortolotti, I. Pérez-Dorado, G. Goñi, M. Medina, J.A. Hermoso, N. Carrillo, N. Cortez, Coenzyme binding and hydride transfer in *Rhodobacter capsulatus* ferredoxin/flavodoxin NADP(H) oxidoreductase, Biochim. Biophys. Acta 1794 (2009) 199–210.
[28] V.J. Hilser, Biochemistry. An ensemble view of allostery, Science 327 (2010) 653–654.
[29] L. Pauling, Chemical achievement and hope for the future, Am. Sci. 36 (1948) 51–58.
[30] R.P. Bell, The Proton in Chemistry, 2nd ed. Chapman and Hall, London, 1973.
[31] R.P. Bell, The Tunnel Effect in Chemistry, Chapman and Hall, London; New York, 1980.
[32] M.J. Knapp, K. Rickert, J.P. Klinman, Temperature-dependent isotope effects in soybean lipoxygenase-1: correlating hydrogen tunneling with protein dynamics, J. Am. Chem. Soc. 124 (2002) 3865–3874.
[33] A. Kohen, R. Cannio, S. Bartolucci, J.P. Klinman, Enzyme dynamics and hydrogen tunnelling in a thermophilic alcohol dehydrogenase, Nature 399 (1999) 496–499.
[34] Z.D. Nagel, J.P. Klinman, A 21st century revisionist's view at a turning point in enzymology, Nat. Chem. Biol. 5 (2009) 543–550.
[35] B.J. Bahnson, T.D. Colby, J.K. Chin, B.M. Goldstein, J.P. Klinman, A link between protein structure and enzyme catalyzed hydrogen tunneling, Proc. Natl. Acad. Sci. U. S. A. 94 (1997) 12797–12802.
[36] D. Borgis, J.T. Hynes, Curve crossing formulation for proton transfer reactions in solution, J. Phys. Chem. 100 (1996) 1118–1128.
[37] D. Antoniou, S. Caratzoulas, C. Kalyanaraman, J.S. Mincer, S.D. Schwartz, Barrier passage and protein dynamics in enzymatically catalyzed reactions, Eur. J. Biochem. 269 (2002) 3103–3112.
[38] W.J. Bruno, W. Bialek, Vibrationally enhanced tunneling as a mechanism for enzymatic hydrogen transfer, Biophys. J. 63 (1992) 689–699.
[39] A.M. Kuznetsov, J. Ulstrup, Proton and hydrogen atom tunneling in hydrolytic and redox enzyme catalysis, Can. J. Chem. 77 (1999) 1085–1096.
[40] M.J. Knapp, J.P. Klinman, Environmentally coupled hydrogen tunneling. Linking catalysis to dynamics, Eur. J. Biochem. 269 (2002) 3113–3121.
[41] S. Hay, N.S. Scrutton, Good vibrations in enzyme-catalysed reactions, Nat. Chem. 4 (2012) 161–168.
[42] V.C. Nashine, S. Hammes-Schiffer, S.J. Benkovic, Coupled motions in enzyme catalysis, Curr. Opin. Chem. Biol. 14 (2010) 644–651.
[43] J.P. Klinman, Importance of protein dynamics during enzymatic C – H bond cleavage catalysis, Biochemistry 52 (2013) 2068–2077.
[44] C.R. Pudney, A. Guerriero, N.J. Baxter, L.O. Johannissen, J.P. Waltho, S. Hay, N.S. Scrutton, Fast protein motions are coupled to enzyme H-transfer reactions, J. Am. Chem. Soc. 135 (2013) 2512–2517.
[45] S.C. Kamerlin, A. Warshel, At the dawn of the 21st century: is dynamics the missing link for understanding enzyme catalysis? Proteins 78 (2010) 1339–1375.
[46] Z.D. Nagel, C.W. Meadows, M. Dong, B.J. Bahnson, J.P. Klinman, Active site hydrophobic residues impact hydrogen tunneling differently in a thermophilic alcohol dehydrogenase at optimal versus nonoptimal temperatures, Biochemistry 51 (2012) 4147–4156.
[47] J. Basran, R.J. Harris, M.J. Sutcliffe, N.S. Scrutton, H-tunneling in the multiple H-transfers of the catalytic cycle of morphinone reductase and in the reductive half-reaction of the homologous pentaerythritol tetranitrate reductase, J. Biol. Chem. 278 (2003) 43973–43982.
[48] A. Sánchez-Azqueta, B. Herguedas, R. Hurtado-Guerrero, M. Hervás, J.A. Navarro, M. Martínez-Júlvez, M. Medina, A hydrogen bond network in the active site of *Anabaena* ferredoxin-NADP$^+$ reductase modulates its catalytic efficiency, Biochim. Biophys. Acta 1837 (2014) 251–263.
[49] D.L. Catalano-Dupuy, D.V. Rial, E.A. Ceccarelli, Inhibition of pea ferredoxin-NADP(H) reductase by Zn-ferrocyanide, Eur. J. Biochem. 271 (2004) 4582–4593.
[50] M.A. Musumeci, A.K. Arakaki, D.V. Rial, D.L. Catalano-Dupuy, E.A. Ceccarelli, Modulation of the enzymatic efficiency of ferredoxin-NADP(H) reductase by the amino acid volume around the catalytic site, FEBS J. 275 (2008) 1350–1366.
[51] M. Martínez-Júlvez, J. Hermoso, J.K. Hurley, T. Mayoral, J. Sanz-Aparicio, G. Tollin, C. Gómez-Moreno, M. Medina, Role of Arg100 and Arg264 from *Anabaena* PCC 7119 ferredoxin-NADP$^+$ reductase for optimal NADP$^+$ binding and electron transfer, Biochemistry 37 (1998) 17680–17691.

[52] M. Medina, M. Martínez-Júlvez, J.K. Hurley, G. Tollin, C. Gómez-Moreno, Involvement of glutamic acid 301 in the catalytic mechanism of ferredoxin-NADP$^+$ reductase from *Anabaena* PCC 7119, Biochemistry 37 (1998) 2715–2728.
[53] V.V. Pollock, M.J. Barber, Kinetic and mechanistic properties of biotin sulfoxide reductase, Biochemistry 40 (2001) 1430–1440.
[54] M.L. Tondo, J. Ottado, E.G. Orellano, Expression, purification and characterization of the ferredoxin-NADP(H) reductase from the phytopathogen *Xanthomonas axonopodis* pv. *citri*, in: S. Frago, M. Medina, C. Gomez-Moreno (Eds.), Flavins and Flavoproteins, Prensas Universitarias de Zaragoza, Zaragoza, 2008, pp. 255–259.
[55] A. Sánchez-Azqueta, M. Martínez-Júlvez, M. Hervás, J.A. Navarro, M. Medina, External loops at the ferredoxin-NADP(+) reductase protein-partner binding cavity contribute to substrates allocation, Biochim. Biophys. Acta 2014 (1837) 251–263.
[56] S. Daff, An appraisal of multiple NADPH binding-site models proposed for cytochrome P450 reductase, NO synthase, and related diflavin reductase systems, Biochemistry 43 (2004) 3929–3932.
[57] A. Sánchez-Azqueta, M.A. Musumeci, M. Martínez-Júlvez, E.A. Ceccarelli, M. Medina, Structural backgrounds for the formation of a catalytically competent complex with NADP(H) during hydride transfer in ferredoxin-NADP$^+$ reductases, Biochim. Biophys. Acta 1817 (2012) 1063–1071.
[58] A. Bortolotti, A. Sanchez-Azqueta, C.M. Maya, A. Velazquez-Campoy, J.A. Hermoso, M. Medina, N. Cortez, The C-terminal extension of bacterial flavodoxin-reductases: involvement in the hydride transfer mechanism from the coenzyme, Biochim. Biophys. Acta 1837 (2014) 33–43.
[59] C.J. Batie, H. Kamin, Association of ferredoxin-NADP$^+$ reductase with NADP(H) specificity and oxidation–reduction properties, J. Biol. Chem. 261 (1986) 11214–11223.
[60] J. Tejero, J.R. Peregrina, M. Martínez-Júlvez, A. Gutiérrez, C. Gómez-Moreno, N.S. Scrutton, M. Medina, Catalytic mechanism of hydride transfer between NADP$^+$/H and ferredoxin-NADP$^+$ reductase from *Anabaena* PCC 7119, Arch. Biochem. Biophys. 459 (2007) 79–90.
[61] J.A. Hermoso, T. Mayoral, M. Faro, C. Gomez-Moreno, J. Sanz-Aparicio, M. Medina, Mechanism of coenzyme recognition and binding revealed by crystal structure analysis of ferredoxin-NADP$^+$ reductase complexed with NADP$^+$, J. Mol. Biol. 319 (2002) 1133–1142.
[62] D.H. Paladini, M.A. Musumeci, N. Carrillo, E.A. Ceccarelli, Induced fit and equilibrium dynamics for high catalytic efficiency in ferredoxin-NADP(H) reductases, Biochemistry 48 (2009) 5760–5768.
[63] J.R. Peregrina, B. Herguedas, J.A. Hermoso, M. Martínez-Júlvez, M. Medina, Protein motifs involved in coenzyme interaction and enzymatic efficiency in *Anabaena* ferredoxin-NADP$^+$ reductase, Biochemistry 48 (2009) 3109–3119.
[64] V.I. Dumit, T. Essigke, N. Cortez, G.M. Ullmann, Mechanistic insights into ferredoxin-NADP(H) reductase catalysis involving the conserved glutamate in the active site, J. Mol. Biol. 397 (2010) 814–825.
[65] J. Sancho, C. Gómez-Moreno, Interaction of ferredoxin-NADP$^+$ reductase from *Anabaena* with its substrates, Arch. Biochem. Biophys. 288 (1991) 231–238.
[66] A. Wang, Y. Zeng, H. Han, S. Weeratunga, B.N. Morgan, P. Moenne-Loccoz, E. Schonbrunn, M. Rivera, Biochemical and structural characterization of *Pseudomonas aeruginosa* Bfd and FPR: ferredoxin NADP$^+$ reductase and not ferredoxin is the redox partner of heme oxygenase under iron-starvation conditions, Biochemistry 46 (2007) 12198–12211.
[67] J.P. Klinman, An integrated model for enzyme catalysis emerges from studies of hydrogen tunneling, Chem. Phys. Lett. 471 (2009) 179–193.